The Astrophysical Journal, 668: L159–L162, 2007 October 20

HIGHLY COLLIMATED JETS AND WIDE-ANGLE OUTFLOWS IN HH 46/47: NEW EVIDENCE FROM *SPITZER* INFRARED IMAGES

T. Velusamy,[1] William D. Langer,[1] and Kenneth. A. Marsh[1,2]
Received 2007 June 29; accepted 2007 August 31; published 2007 October 2

ABSTRACT

We present new details of the structure and morphology of the jets and outflows in HH 46/47 as seen in *Spitzer* infrared images from IRAC and MIPS, reprocessed using the "HiRes" deconvolution technique. HiRes improves the visualization of spatial morphology by enhancing resolution (to subarcsecond levels in IRAC bands) and removing the contaminating side lobes from bright sources. In addition to sharper views of previously reported bow shocks, we have detected (1) the sharply delineated cavity walls of the wide-angle biconical outflow, seen in scattered light on both sides of the protostar, (2) several very narrow jet features at distances ~400 AU to ~0.1 pc from the star, and (3) compact emissions at MIPS 24 μm coincident with the jet heads, tracing the hottest atomic/ionic gas in the bow shocks. Together the IRAC and MIPS images provide a more complete picture of the bow shocks, tracing both the molecular and atomic/ionic gases, respectively. The narrow width and alignment of all jet-related features indicate a high degree of jet collimation and low divergence (width of ~400 AU increasing by only a factor of 2.3 over 0.2 pc). The morphology of this jet, bow shocks, wide-angle outflows, and the fact that the jet is nonprecessing and episodic, constrain the mechanisms for producing the jet's entrained molecular gas, and origins of the fast jet, and slower wide-angle outflow.

Subject headings: ISM: Herbig-Haro objects — ISM: individual (HH 46/47) — ISM: jets and outflows — stars: formation

1. INTRODUCTION

Protostellar jets and winds originate close to the surface of the forming star and interact with the dense envelope surrounding the protostar-disk system (Königl & Pudritz 2000; Shu et al. 2000). Both wide-angle outflows and collimated jets from young protostars play an important role in how stars form, as they provide a means for protostellar disks to shed material and angular momentum, thus regulating stellar mass via accretion of disk material onto the star. HH 46/47 is a remarkable example of a system with jets and bow shock cavities, and, as reported here, wide-angle outflow cavities, offering a rich observational insight into the various mechanisms at play (Reipurth & Heathcote 1991; Chernin & Masson 1991; Eislöffel et al. 1994; Combet et al. 2006). The jets in HH 46/47 are bright and show a classic structure of a collimated flow with several large bow shocks (HH 47A, HH 47C, HH 47D). Recently, the HH 46/47 system was observed by *Spitzer* with the IRAC, IRS, and MIPS instruments as part of the Early Release Observations, and the results were presented by Noriega-Crespo et al. (2004) and Raga et al. (2004). In the IRAC bands, they clearly detect the bow shock and its cavities; these IR emissions arise from the H_2 rotational lines and possibly some contribution from PAHs. However, in these images many of the features in both the IRAC and MIPS data are overwhelmed by the diffraction lobes from the very bright central source. Here we present new results for HH 46/47 based on reprocessing the IRAC and MIPS *Spitzer* archive data using a deconvolution algorithm. The HiRes deconvolution developed for *Spitzer* images by Backus et al. (2005) is based on the Richardson-Lucy algorithm (Richardson 1972; Lucy 1974) and the Maximum Correlation Method (Aumann et al. 1990) used for *IRAS* data. HiRes deconvolution improves the visualization of spatial morphology by enhancing resolution (to subarcsecond levels in the IRAC bands) and removing the contaminating sidelobes from bright sources (Velusamy et al. 2007a, 2007b).

[1] Jet Propulsion Laboratory, Pasadena, CA 91109; velusamy@jpl.nasa.gov.
[2] IPAC, Caltech, Pasadena, CA 91125.

2. RESULTS

In Figures 1–3, we present the HiRes deconvolved images of HH 46/47 in all IRAC bands and in MIPS 24 μm using the data in the *Spitzer* archives. For comparison the diffraction-limited "mosaic" images are also shown in Figure 1. The effects of the resolution enhancement (e.g., from 2.4″ to ~ 0.8″ at 8 μm) and the removal of the diffraction lobes (with residues near the Airy rings at a level <0.05% of the peak intensity) are clearly evident in these images. A wide-angle outflow cavity is now clearly detected in scattered light in the 3.6 and 4.5 μm images, while the bow shocks and their limb-brightened cavities appear prominently in all IRAC bands. At 24 μm, we detect only the central protostar and two compact sources near the tip of the bow shocks (Figs. 1 and 3). In Figure 2 we show a blow-up of the emissions in IRAC channels 1–2 near the protostar. A composite view of the overall morphology and identification of the individual components of the HH 46/47 outflow/jet system is shown in Figure 3. Spectral energy distributions (SEDs) of selected features are shown in Figure 4.

2.1. *Collimated Jets*

The most significant result of our HiRes processing is the jet morphology. In the southwest, we observe well-collimated jet features on all distance scales from the protostar, up to its termination at the head of the bow shock HH 47C (24 μm hot spot). In the northeast the most remarkable jet feature is the 24 μm hot spot at the jet impact site in the bow shock HH 47A. Here we do not observe any other jet emission features toward the bowshock, unlike the case of the southwest jet. The emission features along the southwest jet characterize its collimation and quantify its divergence:

1. Closest to the protostar it appears as a protrusion representing the entrained molecular jet closest to its base (Fig. 2).

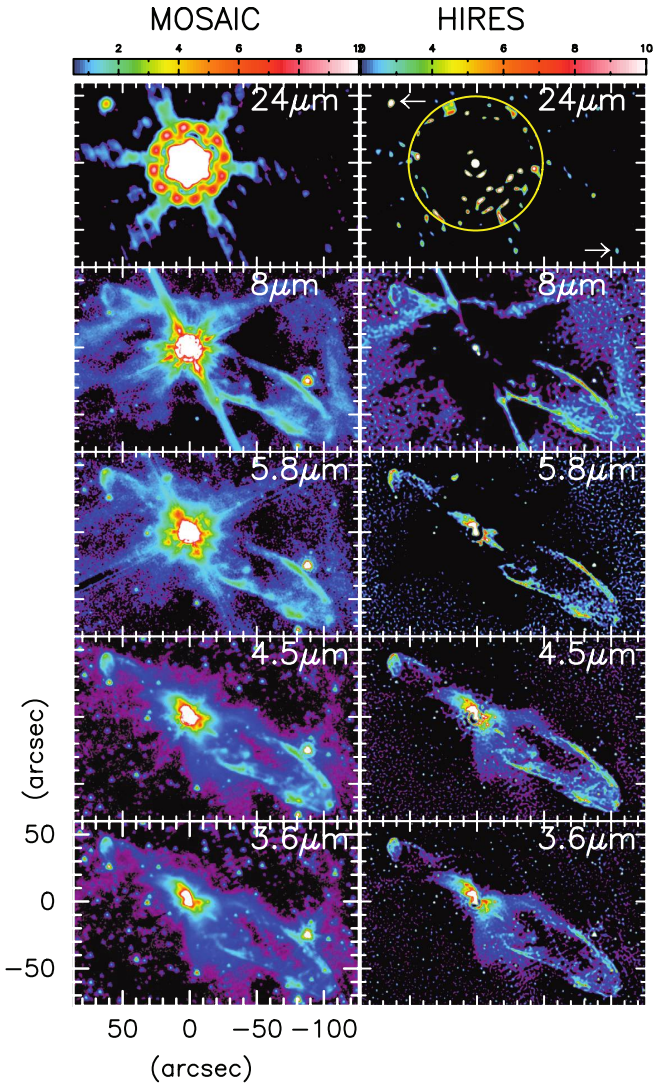

FIG. 1.—Mosaic (*left*) and HiRes deconvolved (*right*) *Spitzer* IRAC and MIPS images of HH 46/47. The intensities are in units of MJy sr^{-1}. Identical square root color stretch is used for all bands such that the low surface brightness is highlighted. The brightest emission in this display (~ 10 MJysr^{-1}) is <1% of the peak in the HiRes images. FWHM of a point source in the HiRes IRAC channels 1–4 is 0.55″–0.75″ and 1.6″ for MIPS 24 μm. The (0, 0) position is R.A. (J2000.0): 08^{h}25^{m}43.68^{s}, decl. (J2000.0) −51°00′34.92″. In the 8 μm image, the northeast-southwest streak is an artifact. In the 24 μm HiRes image, the region inside the circle is confused by diffraction residue below 0.1% of the peak intensity. The white arrows mark the hot spots.

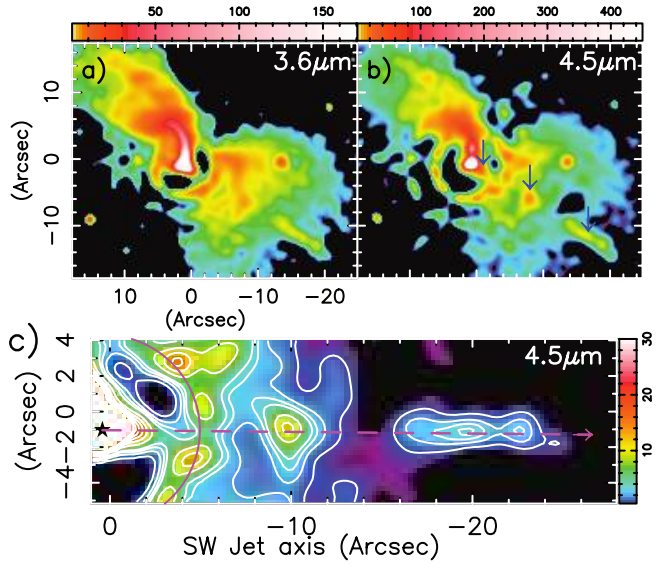

FIG. 2.—(*a*, *b*) HiRes deconvolved images of the region around the protostar (HH 46 IRS) at 3.6 and 4.5 μm. Log color stretch is used with highest intensities at the 20% and 4% levels of the protostar peak brightness at 3.6 and 4.5 μm, respectively. The lowest surface brightness (*blueish green area*) traces the wide-angle outflows to the northeast and southwest. The black arrows in (*b*) mark the jetlike protrusion, H_2 knot, and the compact jet, which are well aligned with the southwest jet (Fig. 3). The circular arc marks the residue in the airy lobe at a level of 0.04% of the peak (1.2 × 10^4 MJy sr^{-1}). (*c*) IRAC 4.5 μm contour map and the gray-scale image of the jet features along the southwest lobe. The contours are at 1, 2, 3, 4, 8, 12, … 32 MJy sr^{-1}. The star symbol and dshed lines mark the protostar and the jet axis.

2. A remarkably very narrow ~1″– 1.5″ wide and ~10″ long "compact jet" (Figs. 2 and 3) is seen at 15″from the protostar. Its long axis is perfectly aligned with the star and 24 μm hot spot (Fig. 3). This feature is also visible in the H_2 images of Eislöffel et al. (1994). Our HiRes IRAC images fully resolve the jet along, and perpendicular to, its velocity axis (Fig. 2*c*). We estimate a radius of ~300 AU for the entrained molecular jet at 9000 AU from the star (at distance 450 pc).

3. A feature ~10″ (4500 AU) from the star is coincident with an optical knot in the *HST* NIC2 image (Reipurth et al. 2000) and a compact feature in the H_2 image (Eislöffel et al. 1994).

4. A feature at ~50″ (0.1 pc) from the star is aligned well with the southwest jet, although we cannot exclude that it is a part of the bow shock seen in projection.

The most prominent jet features in the HiRes 24 μm image are the "hot spots" in the southwest and northeast bow shocks. These emissions were noted in the mosaic images by Noriega-Crespo et al. (2004). Here we discuss their morphology using the HiRes deconvolution and their relationship to the jets and bow shocks. In the IRAC bands the emissions from the bow shocks delineate long arcs that extend to large distances backward from the jet heads to the protostar. The emissions in the IRAC bands are considered to be from pure rotational H_2 lines excited by C-shocks (Neufeld et al. 2006). In contrast, the MIPS 24 μm emissions appear to be coincident with the head of the jets, representing emission generated by shocks in a Working Surface (WS). They are compact and somewhat more extended perpendicular to the jet ~2.2″ × 2.8″ and 3.0″ × 5.9″ axis, sizes for the southwest (HH 47C) and northeast (HH 47A) hot spots, respectively. The morphology of the 24 μm emission (possibly from the J-shock in the WS) is distinctly different from that associated with the molecular shocks (C-shocks) extending farther back. The SEDs of these hot spots show clear 24 μm excess in contrast to that along the bow shock (Fig. 4). The optical (Hartigan et al. 1990) and IR (Noriega-Crespo et al. 2004) spectra in HH 47A show only strong atomic/ionic lines and no continuum. We can therefore rule out the MIPS 24 μm emission as due to warm dust and instead it originates in the hottest gas in the bow shock. In the IRS spectrum of HH 47A (Noriego-Crespo et al. 2004, Fig. 6) bright [Fe II] line emissions at 24.51 and 25.98 μm lie within the MIPS 24 μm passband. Indeed, the faint emission (~ 10 mJy) in the MIPS 24 μm image is consistent with these line intensities, considering the respective widths of the lines and the MIPS 24 μm pass band. Thus, both the northeast and southwest 24 μm hot spots can be regarded as tracing the hottest atomic/ionic gas

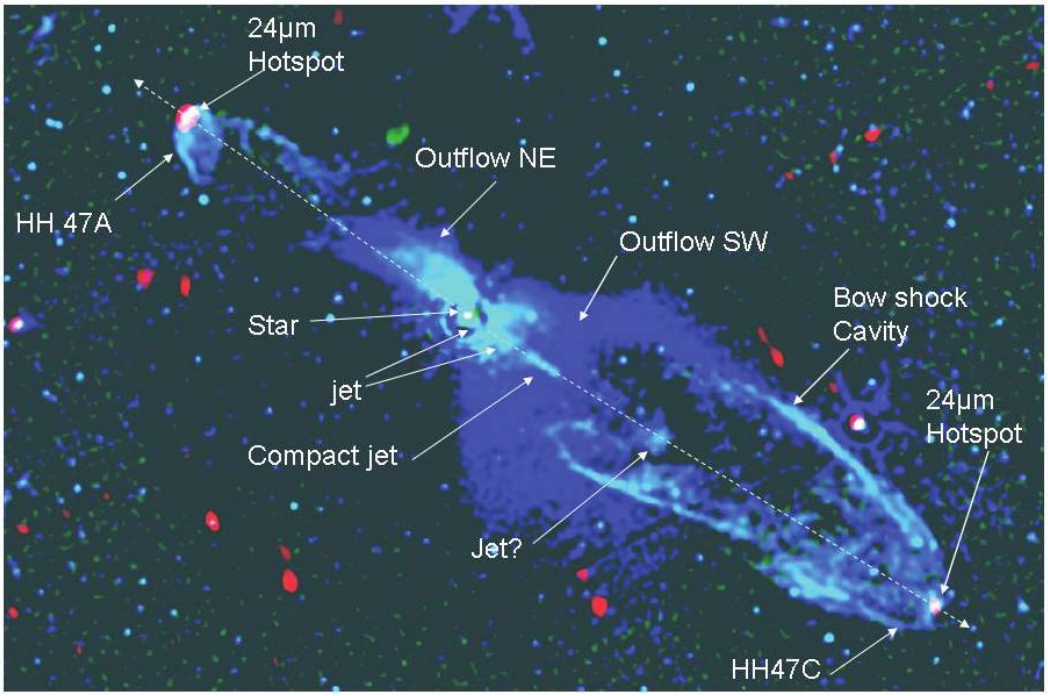

FIG. 3.—HiRes deconvolved three-color *Spitzer* images: IRAC 3.6 μm (*blue*), IRAC (4.5 + 5.8 μm) (*green*), and MIPS 24 μm (*red*). To avoid confusion, the diffraction residue around the protostar in the 24 μm image inside the circle in Fig.1 is not shown. The labels identify the observed features described in the text.

in the bow shocks, and therefore they identify the current impact location of the jet with the ambient envelope.

We use the multiple emission features along the southwest jet to estimate the divergence of the jet. The compact jet at 20″ (9000 AU) from the star has a width of 1.1″ perpendicular to the jet, and the hot spot at a distance of 116″ (0.25 pc) has a width of 2.8″. Taking into consideration the HiRes beams, we estimate the divergence of the jet-entrained molecular material is a factor of ~2.3 over a distance 96″ (~ 0.21 pc). This divergence of the jet (an increase in radius, ~290 AU at 24 μm hot spot), indicates an expansion at 1.8 km s^{-1} perpendicular to the jet, assuming a typical jet velocity of ~250 km s^{-1} (Eislöffel & Mundt 1994). This expansion velocity is consistent with free expansion of the molecular gas transverse to the jet axis at the comoving sound speed (~ 2 km s^{-1} for H_2 at $T_{gas} \sim 10^3$ K). Thus, assuming no external confinement, the jet has remained highly collimated over ~0.2 pc (up to its impact with the surrounding envelope). The spatially discrete emissions along the jet axis suggest that the jet activity is episodic and is consistent with the larger parsec-scale outflows observed in HH 46/47 (Stanke et al. 1999). The alignment of the knots, and the jet head and the linear morphology of the compact jet, rules out a precessing jet.

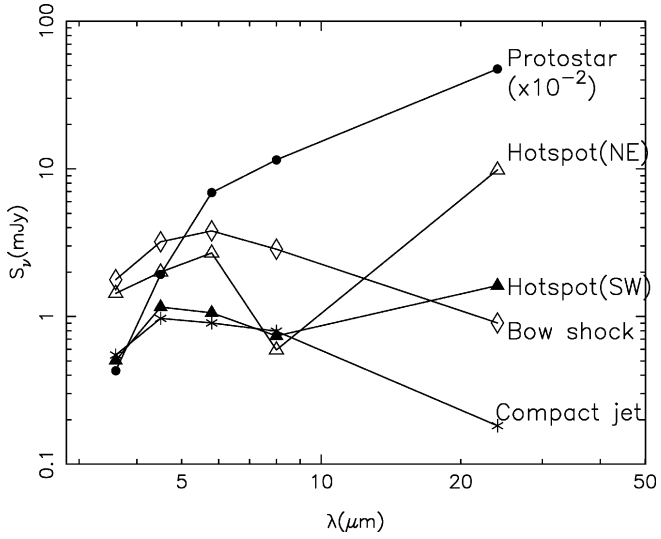

FIG. 4.—SEDs at the positions marked in Fig. 3. The S/Ns for the fluxes are >8 at all positions for all IRAC bands and at the hot spots and protostar for MIPS. The increase in the SED at 24 μm for the hot spots is due to [Fe II] lines in this MIPS band.

2.2. *Wide-Angle Outflows*

The wide-angle outflows are clearly detected in the 3.6 and 4.5 μm HiRes images (Figs. 1–3), and this is the first evidence of a bipolar (northeast and southwest) wide-angle outflow cavity in HH 46/47 as observed in the scattered light from the protostar. The optically observed parabolic sheath of reflection nebulosity toward the northeast (Reipurth et al. 2000) traces parts of this outflow, which is also observed in all IRAC bands. However, the scattered light at 3.6 and 4.5 μm traces a much wider outflow (Figs. 2 and 3). The northeast outflow lobe is clearly a mix of an inner bright parabolic cavity traced in both reflected light and entrained molecular gas, and a broader wide-angle component detected only in scattered light at 3.6 μm. The wide-angle outflow cavity toward the southwest is not detected in the optical, possibly due to its faintness and the viewing geometry, and it may be hidden behind ambient cloud material (Stanke et al. 1999). With this new detection of the wide-angle outflow to the southwest (apparent opening angle of ~110°), HH 46/47 emerges as a classical example of a wide-angle outflow-narrow jet system, placing it among those with very wide outflows (Velusamy & Langer 1998; Arce & Sargent 2006). It would be interesting if such wide opening angles in

HH 46/47 are the result of outflow evolution with age as proposed by Velusamy & Langer (1998). Since outflows can disperse the envelope and modify the infall geometry, this provides a natural mechanism to stop the infall, ending the accreting phase.

3. DISCUSSION

Our HiRes deconvolved *Spitzer* images of HH 46/47 show the concurrent presence of both highly collimated fast bipolar jets and poorly collimated slower wide-angle outflow. The cool molecular gas in the wide-angle outflow (because it does not emit in other IR bands, unlike the jet or the bow shock) is observed along with the presence of warmer entrained molecular gas along the jet close to the protostar (within 1″–2″). The magnetocentrifugal origin of jets and their launch from the magnetized accretion disk of the protostar (Ouyed & Pudritz 1997) are generally accepted, although the detailed mechanism is under debate. In contrast, the wide-angle outflow may be jet-driven (Raga & Cabrit 1993; Ostriker et al. 2001) or wind-driven (Shu et al. 2000). In the jet-driven model the bow shock produces a thin shell that stretches out from the jet head back to the star (Fig. 3). The models of Raga et al. (2004) for HH 47C have a leading bow shock with wings extending all the way back to the protostar, producing a dense shell of material. However, this bow shock bubble is much narrower than the wide-angle outflow traced by scattered light (Fig. 3). Clearly, the wide-angle outflow is not part of this bow shock, and we can rule out a jet-driven origin. The wide-angle outflow alone can be explained by wind-driven models. Another possible scenario for the jet and outflow structure in HH 46/47 is an MHD self-similar model (Lery 2003; Combet et al. 2006) where radiation and magnetocentrifugal acceleration and collimation produce heated pressure-driven outflows. Here, in addition to a central accretion-ejection engine driving the atomic jet, the wide-angle molecular outflow is powered by the infalling matter that follows a circulation pattern around the central object without necessarily being entrained by the jet (Combet et al. 2006, Figs. 4 and 7). The molecular outflows appear as a wider hollow conical structure. The central jet is atomic and occupies the axial region. In this scenario, there is no strong relation between the fast jet and the slower molecular wide-angle outflow near the protostar.

In HH 46/47 the southwest jet is propagating inside a bubble (created by the bow shock), and there is little chance for molecular gas entrainment along its path. Therefore, the detection of the jet features in the molecular gas (IRAC bands) all along the jet axis toward the bow shock indicate that substantial molecular gas entrainment in the jet must have occurred right at the base of the jet. We estimate a size $\sim$ 300 AU for the entrained molecular jet at its base near the star, obtained by extrapolating back to the star the divergence of the molecular jet between the compact jet and the jet head at HH 47C (§ 2.1). In other words, the atomic jet that originates within a few AU of the star must have entrained the molecular gas within the star-disk-infall interface region, which is at least 300 AU across. Thus, our results constrain the density structure above the base of the atomic jet in such a way that sufficient molecular material is still available to the jet to entrain molecular gas across a few hundred AU before it enters the cavity created by the wide-angle outflow and bow shocks. The molecular gas entrainment along the atomic jet occurs at least up to a few hundred AU from the star into the star-disk-infall interface. Such gas entrainment by the jet is possible, for example, in the models by Combet et al. (2006), where the infall-outflow circulation provides a molecular gas buffer over a few hundred AU across and above the star. This material near the vertex of the outflow cones is sufficient for the atomic jet emerging from below to entrain molecular gas as observed in HH 46/47.

We thank the referee for helpful suggestions regarding the interpretation of the 24 μm emission. The research described in this Letter was carried out at the JPL, Caltech, under a contract with NASA. We thank Timothy Thompson for his help with the data analysis.

REFERENCES

Arce, H. G., & Sargent, A. I. 2006, ApJ, 646, 1070
Aumann, H. H., Fowler, J. W., & Melnyk, M. 1990, AJ, 99, 1674
Backus, C. R., Velusamy, T., Thompson, T. J., & Arballo, J. K. 2005, in ASP Conf. Ser. 347, Astronomical Data Analysis Software and Systems XIV, ed. P. Shopbell, M. Britton, & R. Ebert (San Francisco: ASP), 61
Chernin, L., & Masson, C. R. 1991, ApJ, 372, 646
Combet, C., Lery, T., & Murphy, G. C. 2006, ApJ, 637, 798
Eislöffel, J., Davis, C. J., Ray, T. P., & Mundt, R. 1994, ApJ, 422, L91
Eislöffel, J., & Mundt, R. 1994, A&A, 284, 530
Hartigan, P., Raymond, J., & Meaburn, J. 1990, ApJ, 362, 624
Königl, A., & Pudritz, R. E. 2000, In Protostars and Planets IV, ed. V. Mannings, A. P. Boss, & S. S. Russell (Tucson: Univ. Arizona Press), 759
Lery, T. 2003, Ap&SS, 287, 35
Lucy, L. B. 1974, AJ, 79, 745
Neufeld, D. A., et al. 2006, ApJ, 649, 816
Noriega-Crespo, A., et al. 2004, ApJS, 154, 352
Ostriker, E. C., Lee, C., Stone, J. M., & Mundy, L. G. 2001, ApJ, 557, 443
Ouyed, R., & Pudritz, R. E. 1997, ApJ, 482, 712
Raga, A., & Cabrit, S. 1993, A&A, 278, 267
Raga, A. C., Noriega-Crespo, A., Gonzalez, R. F., & Vela¥zquez, P. F. 2004, ApJS, 154, 346
Reipurth, B., & Heathcote, S. 1991, A&A, 246, 511
Reipurth, B., Yu, K., Heathcote, S., Bally, J., & Rodriguez, L. 2000, AJ, 120, 1449
Richardson, W. H. 1972, J. Opt. Soc. Am., 62, 55
Shu, F. H., Najita, J. R., Shang, H., & Li, Z.-Y. 2000, in Protostars and Planets IV, ed. V. Mannings, A. P. Boss, & S. S. Russell (Tucson: Univ. Arizona Press), 789
Stanke, T., McCaughrean, M. J., & Zinnecker, H. 1999, A&A, 350, L43
Velusamy, T., & Langer, W. D. 1998, Nature, 392, 685
Velusamy, T., Langer, W. D., & Marsh, K. A. 2007a, BAAS, 39, 198
Velusamy, T., Marsh, K. A., Beichman, C. A., Backus, C. R., & Thompson, T. J. 2007b, AJ, submitted